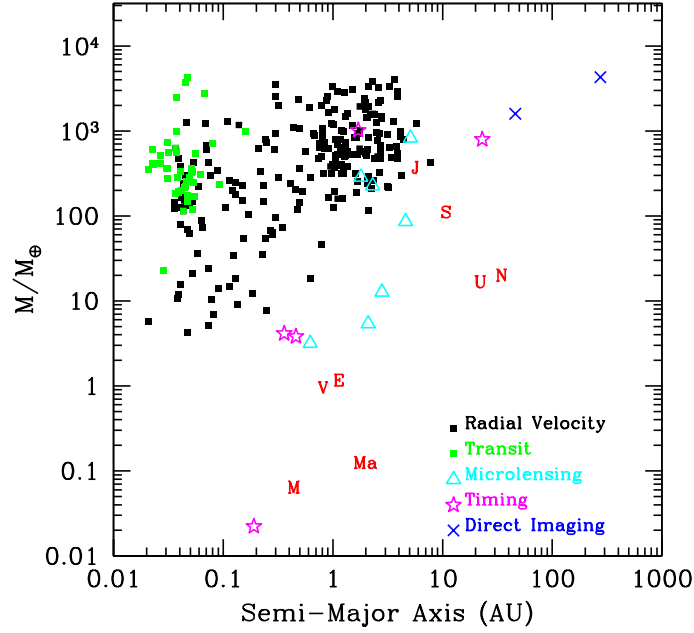


# Transiting Exoplanets with JWST

Seager, S., Deming, D., Valenti, J. A.

**Abstract** The era of exoplanet characterization is upon us. For a subset of exoplanets — the transiting planets — physical properties can be measured, including mass, radius, and atmosphere characteristics. Indeed, measuring the atmospheres of a further subset of transiting planets, the hot Jupiters, is now routine with the *Spitzer Space Telescope*. The *James Webb Space Telescope (JWST)* will continue *Spitzer's* legacy with its large mirror size and precise thermal stability. *JWST* is poised for the significant achievement of identifying habitable planets around bright M through G stars—rocky planets lacking extensive gas envelopes, with water vapor and signs of chemical disequilibrium in their atmospheres. Favorable transiting planet systems, are, however, anticipated to be rare and their atmosphere observations will require tens to hundreds of hours of *JWST* time per planet. We review what is known about the physical characteristics of transiting planets, summarize lessons learned from *Spitzer* high-contrast exoplanet measurements, and give several examples of potential *JWST* observations.



**Fig. 1** Known planets as of July 2008. We have defined planet to have a maximum mass of 13 Jupiter masses. The symbols indicate the discovery technique; see text for details. Data from [1].

## 1 Introduction

The existence of exoplanets is firmly established with over 300 known to orbit nearby, sun-like stars. Figure 1 shows the known exoplanets as of July 2008 with symbols indicating their discovery techniques [1]. The majority of the known exoplanets have been discovered by the Doppler technique which measures the star's line-of-sight motion as the star orbits the planet-star common center of mass [2, 3]. While most planets discovered with the Doppler technique are giant planets, the

---

S. Seager

Dept. of Earth, Atmospheric, and Planetary Sciences, Dept. of Physics, Massachusetts Institute of Technology, 77 Massachusetts Ave., 54-1626, Cambridge, MA, 02139 e-mail: seager@mit.edu

D. Deming

NASA/Goddard Space Flight Center, Planetary Systems Branch, Code 693 Greenbelt, MD 20771 e-mail: leo.d.deming@nasa.gov

J. A. Valenti

Space Telescope Science Institute, 3700 San Martin Dr., Baltimore, MD 21218 e-mail: valenti@stsci.edu

new frontier is discovery of super Earths (loosely defined as planets with masses between 1 and  $10 M_{\oplus}$ ). About a dozen radial velocity planets with  $M < 10 M_{\oplus}$  and another dozen with  $10 M_{\oplus} < M < 30 M_{\oplus}$  have been reported. The transit technique finds planets by monitoring thousands of stars, looking for the small drop in brightness of the parent star that is caused by a planet crossing in front of the star. At the time of writing this article, around 50 transiting planets are known. Due to selection effects, transiting planets found from ground-based searches are limited to small semi-major axes [4]. Gravitational microlensing has recently emerged as a powerful planet-finding technique, discovering 6 planets, two belonging to a scaled down version of our own solar system [5]. Direct imaging is able to find young or massive planets with very large semi-major axes. The mass of directly imaged planets (e.g., [6] and references therein) is inferred from the measured flux based on evolution models, and is hence uncertain. The timing discovery method includes both pulsar planets [7] and planets orbiting stars with stable oscillation periods [8].

Many fascinating properties of exoplanets have been uncovered by the initial data set of hundreds of exoplanets. A glance at Figure 1 shows one of the most surprising features: that exoplanets exist in an almost continuous range of mass and semi-major axis. Not shown in Figure 1 are the equally wide range of eccentricities; several different theories for the origin of planet eccentricities have been proposed. Because there is not enough solid material close to the star in a protoplanetary disk, the giant planets are believed to have formed further out in the disk and migrated inwards. The migration stopping mechanisms, and even the details of planet migration are not fully understood. Out of the  $\sim 50$  known transiting exoplanets, several have very large radii, and are too big for their mass and age according to planet evolution models (see Figure 5). These “puffed-up” planets must have extra energy in their core that prevents cooling and contraction, but no satisfactory explanation yet exists.

The next step beyond discovery is to characterize the physical properties of exoplanets by measuring densities, atmospheric composition, and atmospheric temperatures.

There are two paths to exoplanet characterization. The first is direct imaging where the planet and star are spatially separated on the sky. Direct imaging has been successful for discovering hot or massive planetary candidates with large ( $\sim 50$ – $100$  AU) orbital and projected spatial separation [6, 9, 10]. Although *JWST* will incorporate several coronagraphic modes, neither the telescope nor the instruments were optimized for coronagraphy. A relatively large inner working angle and limited planet-star contrast restrict *JWST* to studying young or massive Jupiters with large semi-major axes. The case for *JWST* coronagraphic observations of exoplanets is presented in [11].

Solar-system aged small planets are not observable via direct imaging with current technology, even though an Earth at 10 pc is brighter than the faintest galaxies observed by the *Hubble Space Telescope* (*HST*). The major impediment to direct observations is instead the adjacent host star; the Sun is 10 million to 10 billion times brighter than Earth (for mid-infrared and visible wavelengths, respectively). No existing or planned telescope is capable of achieving this contrast ratio at 1 AU separations.

The second path to exoplanet characterization is via the transit technique. A subset of exoplanets cross in front of their stars as seen from Earth (“primary eclipse” or “transit”). Planets that cross in front of their star, also pass behind the star (secondary eclipse), provided that the transiting planet is on a circular orbit. The probability to transit is  $\sim R_*/a$ , where  $R_*$  is the stellar radius and  $a$  the semi-major axis. Transits are therefore most easily found for planets orbiting close to the star. Indeed, all but one of the  $\sim 50$  known transiting exoplanets have  $a < 0.09$  AU (See [1] and references therein).

Observations of transiting planets exploit separation of photons in time, rather than in space (see Figure 2). That is, observations are made in the combined light of the planet-star system. When the planet transits the star as seen from Earth the starlight gets dimmer by the planet-to-star area ratio. If the size of the star is known, the planet size can be derived. During the planet transit, some of the starlight passes through the optically thin part of the planet atmosphere, picking up spectral features from the planet. A planetary transmission spectrum can be obtained by dividing the spectrum of the star and planet during transit by the spectrum of the star alone (the latter taken before or after transit).

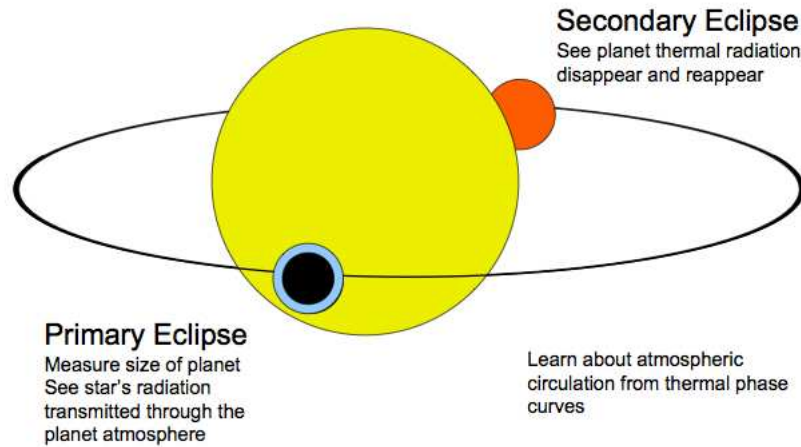


**Fig. 2** Schematic of a planet transit. Not to scale.

When the planet disappears behind the star, the total flux from the planet-star system drops. The drop is related to both relative sizes of the planet and star and their relative brightnesses (at a given wavelength). The flux spectrum of the planet can be derived by subtracting the flux spectrum of the star alone (during secondary eclipse) from the flux spectrum of both the star and planet (just before and after secondary eclipse). The planet's flux gives information on the planet composition and temperature gradient (at infrared wavelengths) or albedo (at visible wavelengths). Finally, non-transiting exoplanets can in principle also be observed in the combined

planet-star flux as the planet goes through illumination phases as seen from Earth. In the thermal infrared the phase observations provide information on energy redistribution of absorbed stellar radiation (see Section 2.3) and at visible wavelengths the phase observations give information on scattering particles (gas or clouds).

Primary and secondary eclipses enable high-contrast measurements because the precise on/off nature of the transit and secondary eclipse events provide an intrinsic calibration reference. This is one reason why the *Hubble Space Telescope* and the *Spitzer Space Telescope* have been so successful in measuring high-contrast transit signals that were not considered in their designs.

## 2 *Spitzer's* Legacy

### 2.1 Background

The *Spitzer* Space Telescope is a cryogenically cooled 85 cm diameter telescope launched into an Earth-trailing orbit in 2003. All three of *Spitzer's* science instruments (IRAC [12], IRS [13], and MIPS [14]) have been used to study exoplanets. *Spitzer* has revolutionized the field of exoplanets by making measurements of hot Jupiter atmospheres routine. The *Spitzer* exoplanet studies are directly relevant to *JWST* because *JWST* will make similar measurements, but with much higher S/N, for much smaller exoplanets, or for planets with semi-major axes beyond 0.05 AU.

We describe one reason why *Spitzer* has been so successful in detecting photons from exoplanets during secondary eclipse. Figure 3 shows the relative fluxes for the Sun, Jupiter, Earth, Venus, and Mars, approximating each as a black body. The planets also reflect light from the Sun at visible wavelengths, giving them two flux peaks in their schematic spectrum. We see from Figure 3 that at infrared wavelengths ( $< 10\mu\text{m}$ ) the solar system planets are more than 7 orders of magnitude fainter than the Sun. A generic hot Jupiter, with assumed geometric albedo of 0.05, equilibrium temperature of 1600 K, and a radius of  $1.2 R_J$  is also shown on the same figure. This representative hot Jupiter is less than 3 orders of magnitude fainter than the Sun at some wavelengths. Equally important is that the planet-to-star flux ratio is favorable where the star and planet flux are high, i.e. plenty of photons are available to reach the telescope. The  $\sim 8\mu\text{m}$  region is therefore a sweet spot for *Spitzer* observations of hot Jupiter exoplanets.

### 2.2 Exoplanet Radii

A precise planet radius together with planet mass enables a study of the planet's density and interior bulk composition. We have shown that infrared wavelengths are ideal for deriving a precise planet radius from the transit light curve, due to the

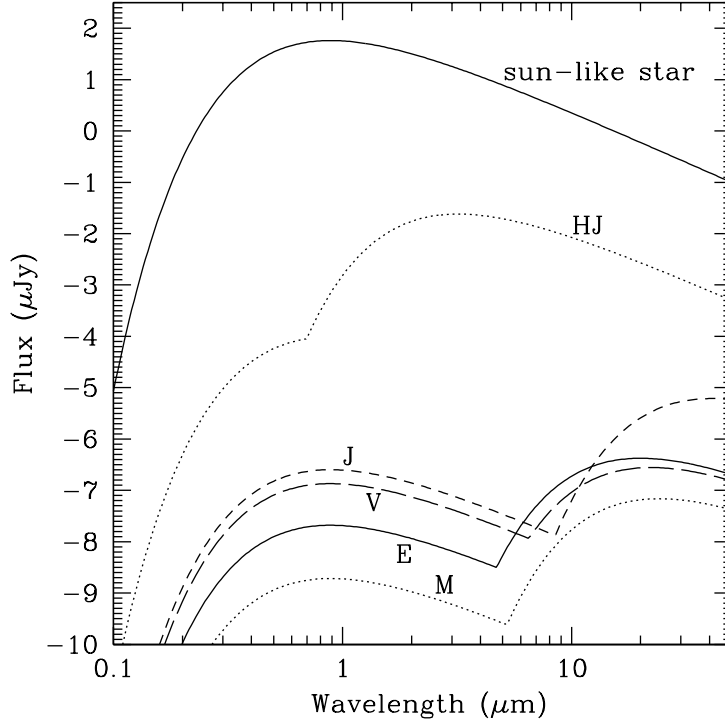


**Fig. 3** Black body flux (in units of  $10^{-26} \text{ W m}^{-2} \text{ Hz}^{-1}$ ) of some solar system bodies as “seen” from 10 pc. The Sun is represented by a 5750 K black body. The planets Jupiter, Venus, Earth, and Mars are shown and are labeled with their first initial. A putative hot Jupiter is labeled with “HJ”. The planets have two peaks in their spectra. The short-wavelength peak is due to sunlight scattered from the planet atmosphere and is computed using the planet’s geometric albedo. The long-wavelength peak is from the planet’s thermal emission and is estimated by a black body of the planet’s effective temperature. Data from [20]. The Hot Jupiter albedo was assumed to be 0.05 and the equilibrium temperature to be 1600 K.

miniscule amount of stellar limb darkening at infrared wavelengths [15]. In contrast, at visible wavelengths limb darkening affects the shape of the transit light curve. Because limb darkening is imperfectly known for stars other than the Sun, limb darkening must be solved for from planet transit light curves at visible wavelengths in order to fit the planet’s radius. *Spitzer* measurements of the HD 209458 primary eclipse with MIPS at  $24 \mu\text{m}$  yielded a planetary radius of  $1.26 \pm 0.08 R_J$  [15]. At shorter infrared wavelengths with more photons from the star and where limb darkening is still negligible, and for host stars of later spectral type than HD 209458, transit light curves will enable even more precise planet radii to be derived.

Transit observations at infrared wavelengths are especially useful for planets transiting M stars. M stars are faint at visible wavelengths with peak flux output at near-IR wavelengths. *Spitzer* is arguably the best existing telescope for determin-

ing precise radii of planets transiting M stars. The Neptune-mass planet GJ 436b [16, 17] was observed by *Spitzer* to have a Neptune-like radius of  $4.33 \pm 0.18 R_{\oplus}$  [18, 19].

### 2.3 Exoplanet Atmosphere Summary

Several different exoplanets have published *Spitzer* secondary eclipse atmosphere measurements. These secondary eclipse measurements have detection significances ranging from  $60\sigma$  [21] down to  $5\sigma$ . Rather than describe each planet individually, we present a summary based on an important question related to atmospheric circulation.

Hot Jupiters are expected to be tidally locked to their parent stars—presenting the same face to the star at all times. This causes a permanent day and night side. A long standing question has been about the temperature difference from the day to night side. Are the hot Jupiters scorchingly hot on the day side and exceedingly cold on the night side? Or, does atmospheric circulation efficiently redistribute the absorbed stellar radiation from the day side to the night side?

Surprisingly, *Spitzer* has found that both scenarios are possible. *Spitzer* has measured the flux of the planet and star system as a function of orbital phase for several hot Jupiter systems [23, 24, 21]. Assuming that the star is constant in flux, the resulting brightness change is due to the planet alone. The HD 189733 star and planet shows some variation at  $8 \mu\text{m}$  during the 30 hour continuous observation of half an orbital phase [21]. This variation corresponds to about 20% variation in planet temperature (from a brightness temperature of 1212 to 973 K). In contrast, the non-transiting exoplanet *Uranus* shows a marked day-night contrast suggesting that the day and night side temperatures differ by over 1000 K [23].

Once the stellar radiation is absorbed on the planet’s day side, there is a competition between reradiation and advection. If the radiation is absorbed high in the atmosphere, the reradiation timescale is short and reradiation dominates over advection. In this case the absorbed stellar radiation is reradiated before it has a chance to be advected around the planet, resulting in a very hot planet day side and a correspondingly very cold night side. If the radiation penetrates deep into the planet atmosphere where it is finally absorbed, the advective timescale dominates and the absorbed stellar radiation is efficiently circulated around the planet. This case would generate a planet with a small temperature variation around the planet. See also [25, 26, 27, 28]. See [29] and references therein for a review discussion of atmospheric circulation models.

In Figure 4 we plot measured brightness temperatures of seven hot exoplanets together with two equilibrium temperature ( $T_{eq}$ ) curves. One of the  $T_{eq}$  curves is for a planet with evenly redistributed absorbed stellar radiation ( $f = 1/4$  below), corresponding to a planet with little temperature difference between the day and night sides. The other  $T_{eq}$  curve is for a planet with instantaneous reradiation of absorbed stellar radiation ( $f = 2/3$  below), corresponding to a planet with a strong

day-night temperature difference. The cooler of the hot exoplanets in Figure 4 lie along the evenly redistributed energy curve, while the hotter exoplanets lie nearer to the instantaneous reradiation  $T_{eq}$  curve.

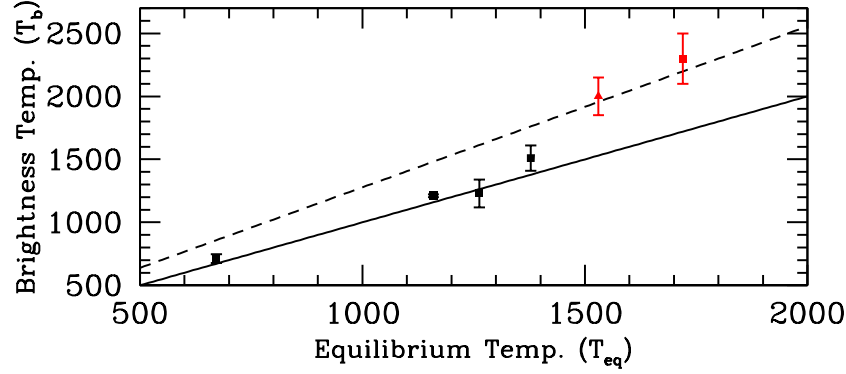


**Fig. 4** Brightness temperature ( $8 \mu\text{m}$ ) as a function of the day side equilibrium temperature for six hot Jupiters. Brightness temperature is the measured flux converted to a temperature. The day side equilibrium temperature  $T_{eq}$ , is defined in equation (1) and the accompanying text. The parameter  $f$  is used to approximate atmospheric circulation: in this formulation of equation (1),  $f = 1/4$  corresponds to a uniform temperature around the planet (solid line), whereas  $f = 2/3$  corresponds to instantaneous reradiation on the planet’s dayside hemisphere (dashed line). The cooler planets lie near the uniform temperature line whereas the hotter planets lie near the hot day side line. From left to right, the brightness temperatures are GJ 436b [18], HD 189733 b [21], TrES-1 [31], HD 209458b [33], Ups And [23], HD 149026 [26]. (Note that the Ups And day side temperature is estimated from its thermal phase curve).

Physically,  $T_{eq}$  is the effective temperature attained by an isothermal planet after it has reached complete equilibrium with the radiation from its parent star.  $T_{eq}$  is described by

$$T_{eq} = T_* \left( \frac{R_*}{a} \right)^{1/2} [f(1 - A_B)]^{1/4}, \quad (1)$$

where  $T_*$  and  $R_*$  are the effective temperature and the radius of the star,  $a$  is the planet semi-major axis, and  $f$  and  $A_B$  are the re-radiation factor and the Bond albedo of the planet.

Here we explain how hot Jupiters can exist both with and without large day-night temperature variations. See also [30, 26, 27, 28]. Hot planets such as Ups And are on one side of a temperature-driven chemical composition boundary, while cooler planets such as HD 209458b are on the cooler side. Specifically, if the hot Jupiter planet atmosphere is relatively cool, TiO is locked into solid particles that have little absorbing power in the atmosphere. In the hotter atmosphere, TiO is a “deadly” gas that absorbs so strongly it puts the planet in the reradiation regime leading to a large day-night contrast. At the temperature of these hot day side exoplanets, some



elements will be in atomic (instead of molecular) form and atomic line opacities may also play a significant absorbing role.

What evidence do we have for the temperature-induced two-atmosphere hypothesis? Cool stars (M stars) have visible-wavelength spectra that are dominated—and indeed dramatically suppressed—by TiO gas. Hot brown dwarfs also have spectra with TiO absorption features whereas cooler brown dwarfs do not, implying that for cooler brown dwarfs Ti is sequestered in solid particles. Temperature and pressures in hot Jupiter atmospheres are similar to brown dwarfs (although the temperature gradient is different) so that we expect a similar temperature-induced chemical composition.

Other notable exoplanet atmosphere discoveries by *Spitzer* come from spectrophotometry and include discovery of a temperature inversion on the day side of HD 209458b [32, 33] and a tentative detection of water vapor in transmission spectra during primary transit [34, 35].

This interesting “two types of hot Jupiter atmospheres” hypothesis shows just how complex hot Jupiters are. The results also imply that 3D coupled radiative transfer-atmospheric circulation models are needed to fully understand hot Jupiters. Next generation data with *JWST* (Section 4) in terms of high SNR low-resolution spectra as a function of orbital phase will lead to a deeper understanding of hot Jupiter atmospheres.

## 2.4 Lessons Learned from *Spitzer*

*Spitzer* and its instruments were not designed for high contrast observations. Here we describe some of the instrumental effects that become important at the part-per-thousand level and consequently affect exoplanet observations. These may be useful to consider when planning *JWST* exoplanet transit observations.

The most notable instrumental effect is the “ramp”: a gradual detector-induced rise of up to 10% in the signal measured in individual pixels over time. This rise is illumination-dependent; pixels with high levels of illumination converge to a constant value within the first two hours of observations and lower-flux pixels increase linearly over time. [21] have attributed this to charge trapping.

The ramp is present at the long wavelength detectors (8 and 16  $\mu\text{m}$  and possibly also at 5  $\mu\text{m}$ ). The charge trapping is likely caused by the ionized impurities in the arsenic-doped silicon detector. The first electrons that are released by photons get trapped by the ions and therefore they are not immediately read out.

The ramp can be removed from a data set by a fitting a linear plus logarithmic function. A method to avoid the ramp is to “preflash” the detector before an observation, by observing a bright star. We note that at 24  $\mu\text{m}$  no ramp effect is observed [22]; this may be because the detector is always illuminated by the zodiacal background. The ramp effect may be important for *JWST* observations because similar detector materials are being used on MIRI. We recommend pre-flashing before transit observations.

A second instrumental effect that is significant for exoplanet transit observations is the IRAC intrapixel sensitivity variation for the short-wavelength channels (3.5 and 4.5  $\mu\text{m}$ ) [36]. This intrapixel sensitivity variation is a property of the detector, is spatially asymmetric, and does not change with time. One possible explanation of this detector effect is that there are physical gaps between the pixels which are unresponsive to light. When an image is centered on a pixel the highest sensitivity arises. A second possibility is related to the bump-bond contact between the detector and the underlying multiplexer. Each pixel makes electrical contact with the multiplexer at pixel center. In this scenario, the electrons generated close to the contact point may be collected more efficiently than electrons generated at pixel edges. The IRAC intrapixel sensitivity variation can be corrected for by a natural mapping of the pixels, by exploiting the telescope pointing jitter [37].

A third significant instrumental effect found from exoplanet observations is a telescope pointing oscillation with a period of roughly one hour. This pointing oscillation affects IRS slit spectra. As the star becomes uncentered and recentered on the slit the number of photons going through the slit changes. This change is wavelength-dependent, because of the wavelength-dependent PSF, and therefore can generate erroneous features in an exoplanetary spectrum. The cause of the pointing oscillation is still a matter of debate.

A fourth effect is a longer-term telescope drift in telescope pointing. This telescope drift is less certain than the well-documented 1 hour oscillation. This affects the IRS spectral flux in terms of the broad distribution of energy, because the slit width is comparable to the diffraction width of the telescope PSF. This is also a wavelength-dependent effect.

Despite not being designed for high-contrast observations, *Spitzer* has revolutionized the study of exoplanet atmospheres by routinely detecting secondary eclipses of hot Jupiters and measuring their brightness temperatures at different wavelengths. Because of *JWST*'s larger mirror diameter and higher spectral resolution, and by taking care to understand and remove instrumental effects, transit observations with *JWST* hold even more promise.

### 3 Transiting Planet Radii with JWST

*JWST* will continue to study the physical characteristics of transiting exoplanets in the tradition of *Spitzer*. See Chapter 1 of this volume for the *JWST* telescope, instrument, and performance. *JWST* has 40 times the collecting area of *Spitzer*, enabling studies of smaller exoplanets—pushing down to potentially habitable exoplanets.

The overall goal of planet transit observations is to combine the radius with the planet mass to infer an interior bulk composition. Figure 5 shows transiting exoplanets on a mass-radius diagram with curves for planets of homogeneous composition. For example, we would like to know if planets in the mass range 5 to 20  $M_{\oplus}$  have significant gas envelopes like Neptune ( $\sim 10\%$  by mass), or instead consist almost

entirely of rock/iron. Owing to high temperatures at a deeply submerged surface, the former are not habitable, while the latter are.

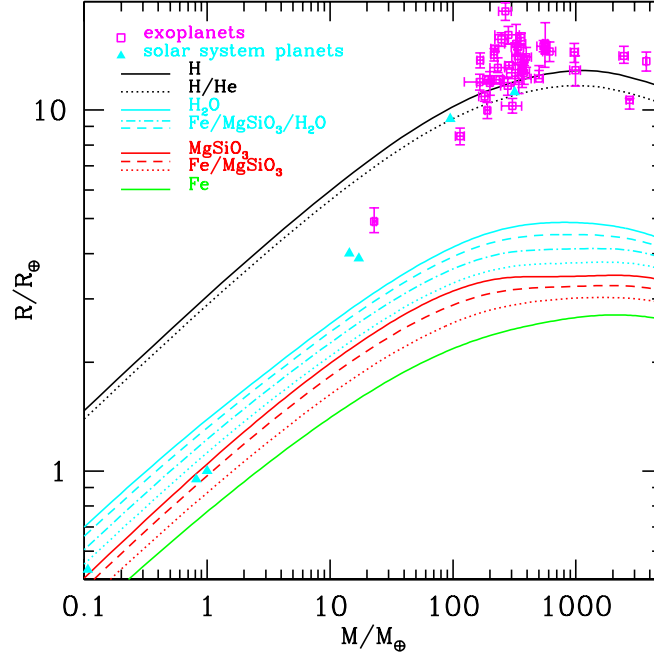


**Fig. 5** Mass-radius relationships for solid planets. The solid lines are models of homogeneous planets. From top to bottom the homogeneous planets are: hydrogen (cyan solid line); a hydrogen-helium mixture with 25% helium by mass (cyan dotted line); water ice (blue solid line); silicate ( $\text{MgSiO}_3$  perovskite; red solid line); and iron ( $\text{Fe}$ ); green solid line). The non-solid lines are models of differentiated planets. The red dashed line is for silicate planets with 32.5% by mass iron cores and 67.5% silicate mantles (similar to Earth) and the red dotted line is for silicate planets with 70% by mass iron core and 30% silicate mantles (similar to Mercury). The blue dashed line is for water planets with 75% water ice, a 22% silicate shell and a 3% iron core; the blue dot-dashed line is for water planets with 45% water ice, a 48.5% silicate shell and a 6.5% iron core (similar to Ganymede); the blue dotted line is for water planets with 25% water ice, a 52.5% silicate shell and a 22.5% iron core. The blue triangles are solar system planets: from left to right Mars, Venus, Earth, Uranus, Neptune, Saturn, and Jupiter. The magenta squares denote the transiting exoplanets, including HD 149026b at  $8.14 R_\oplus$  and GJ 436b at  $3.95 R_\oplus$ . Note that electron degeneracy pressure becomes important at high mass, causing the planet radius to become constant and even decrease for increasing mass. From [38].

To illustrate why precise radii are needed to constrain a planet's mass we show the range of interior compositions possible for a  $10 M_\oplus$ ,  $2 R_\oplus$  planet on a ternary diagram (Figure 6). For an explanation of ternary diagrams in this context see [39] and [40]. There is a degeneracy in interior composition for a solid exoplanet made of the three typical planetary materials: an iron core, silicate mantle, and water outer layer.

This is because of the very different densities of the three components. For example, a planet of a given mass and composition could have the same radius if some of the silicate were exchanged for a combination of water and iron. By showing contour curves of growing observational uncertainties, Figure 6 emphasizes how a precise radius reduces the interior composition uncertainty.

**Fig. 6** A ternary diagram for a planet of a fixed mass and radius, including the mass and radius uncertainties. This example is for a planet with  $M_p = 10 \pm 0.5 M_\oplus$  and  $R_p = 2 \pm 0.1 M_\oplus$ , showing the 1-, 2- and 3- $\sigma$  uncertainty curves as indicated by the color bar. Notice that considering the 3- $\sigma$  uncertainties almost the entire ternary diagram is covered—in other words there is little constraint on the planet internal composition. See [40] for a discussion of the direction and spacing of the curves, as well as for other examples.

*JWST* should be able to measure precise transit light curves for a wide range of star brightnesses. With its spectral dispersion and high cadence observing, NIRSpec will be capable of high-precision spectrophotometry on bright stars. NIRSpec data can then be used in the same way that the *HST* STIS spectra data for HD209458 was rebinned into “photometry” [41]. For fainter M stars, NIRCams should be sufficient. For all stars, the near infrared is ideal because of negligible stellar limb darkening, removing one of the uncertainties in deriving an accurate planet radius from a planet transit light curve.

By scaling from the [41] *HST* data, we provide two interesting examples of *JWST* precision radii [42, 43] with NIRSpec at  $0.7 \mu\text{m}$ . For the first example we consider *Kepler* Earth-size planet candidates orbiting Sun-like stars in 1 AU orbits. *Kepler* stars are about 300 pc distant and Earth-analogs have a transit duration of about 8 hours. With high-cadence observing, *JWST* will be able to obtain a 35- $\sigma$  transit

detection for *Kepler* Earth-analog planet candidates. This *JWST* confirmation would be very significant, because *Kepler*'s SNR detection is 7 over 4 binned transits [44].

A second example is that of an Earth-sized moon orbiting the transiting giant planet HD 209458b. At 47 pc and with a 3 hour transit time (and 6 hour observation), *JWST* will also be capable of a moon transit detection at  $35\text{-}\sigma$  SNR.

## 4 Transiting Planet Atmospheres with *JWST*

### 4.1 Background

Transiting exoplanets present two different configurations for atmosphere measurements. The first is during primary transit and is called transit transmission spectra (described in Section 1). Transmission spectra probe the planetary upper atmosphere and have been used to detect atomic and molecular features in two different exoplanet atmospheres (HD 209458b and HD 189733b), including sodium [45], water vapor [34, 46], and methane [46]. Additionally, [47] have detected a large envelope of atomic hydrogen (and a tentative detection of other elements) indicating a slow atmospheric escape. [48] have presented the first ground-based detection of an exoplanet atmosphere via sodium in HD 189733b.

The magnitude of the transmission spectra signal can be estimated by the area of the planetary atmosphere compared to the area of the star. The area of the planetary atmosphere is an annulus with a radial height of about  $5 \times H$ . Here  $H$  is the planetary scale height

$$H = \frac{kT}{\mu_m g}, \quad (2)$$

where  $k$  is Boltzmann's constant,  $T$  is temperature,  $\mu_m$  is the mean molecular mass, and  $g$  is the planet's surface gravity. The magnitude of the planet transmission spectra signature is approximately

$$5 \times \frac{2R_p H}{R_*^2}, \quad (3)$$

where  $R_p$  is the planet's radius and  $R_*$  is the star's radius. A hot Jupiter's transmission spectra signature is approximately  $10^{-4}$ . We further note that, from the planet's equilibrium effective temperature (equation (1))  $T \sim 1/\sqrt{a}$  so that

$$\text{Transmission} \sim \frac{1}{\sqrt{a}}. \quad (4)$$

We emphasize a very critical difference between planets with hydrogen-rich atmospheres (including both the upper layers of giant planet envelopes and thinner atmospheres of super Earths) and terrestrial planets (including Earths or super Earths) with relatively thin  $\text{N}_2$  or  $\text{CO}_2$  atmospheres. The factor  $\mu_m$  is 2 for an  $\text{H}_2$  atmosphere, but 44 for a  $\text{CO}_2$  atmosphere! Hence, the difference in transmission spec-

tra between hydrogen-rich atmospheres and terrestrial-like planet atmospheres is a factor of 20 (with  $T$  and  $g$  being equal; see [49] for further discussion). This implies that, while smaller space telescopes can study hydrogen-rich exoplanet atmospheres, *JWST*'s 6.5 m effective mirror diameter is needed to study  $\text{CO}_2$ - or  $\text{N}_2$ -dominated atmospheres similar to terrestrial planet atmospheres in our solar system.

The second configuration available for transiting atmosphere studies with *JWST* is secondary eclipse. Observations during secondary eclipse measure the planet's thermal emission. This contains information about the planet's temperature and temperature gradient. Spectral features can also be detected with the planet's thermal emission flux. If absorption lines are detected, the planet has a temperature that is decreasing towards the top of the atmosphere. If emission lines are detected, the planet has a temperature that is increasing towards the top of the atmosphere.

Estimating the magnitude of the planet's thermal emission (in the form of a planet-to-star flux ratio) is not easy because planet model atmospheres are usually needed. That said, we can bracket an estimate with two extremes. One extreme is the case where the thermal emission spectra could be observed over a broad infrared wavelength range to estimate the "bolometric" planet flux. In this case, we can estimate the planet-star flux ratios by a ratio of black bodies, and considering the Stefan-Boltzmann law  $F = \sigma_R T^4$ ,

$$\text{Emission} \sim \frac{R_p^2 T_p^4}{R_*^2 T_*^4}, \quad (5)$$

where we have written  $T_p = T_{eq}$ . Again using the scaling relation  $T_p \sim 1/\sqrt{a}$ , we find

$$\text{Emission} \sim \frac{1}{a^2}. \quad (6)$$

As a separate extreme to estimate the thermal emission planet-star contrast ratio, we can take the Rayleigh-Jeans tail of the black body spectrum  $h\nu \ll kT$  to get

$$\text{Emission} = \frac{R_p^2 T_p}{R_*^2 T_*}, \quad (7)$$

and again using the  $T_{eq} \sim 1/\sqrt{a}$  scaling,

$$\text{Emission} \sim \frac{1}{\sqrt{a}}. \quad (8)$$

More reasonably, we can assume that at the peak of the planet's output, which is neither represented by the bolometric flux nor is it in the Rayleigh-Jeans tail (see Figure 3), the dependence with  $a$  falls between that of  $\sim 1/a^2$  (equation (6)) and  $\sim 1/\sqrt{a}$  (equation (8)).

We have gone through these estimates to make a single main point: a comparison between the semi-major axis ( $a$ ) dependence of transmission and emission spectra. Emission spectra have a stronger signal than transmission spectra for planets orbiting close to their parent stars (and indeed emission spectra are only possible for

planets close to their stars). While transmission spectra are weaker than emission spectra for planets close to their stars, they are still attainable for planets orbiting far from their stars.

## 4.2 Giant Planet Atmospheres

The *JWST* thermal IR detection capability can be explored by scaling the *Spitzer* results (this discussion is from [43]). The 5–8  $\mu\text{m}$  range is ideal for solar-type stars because the planet-star contrast is high and the exo-zodiacal background is low. For an estimate we can take the TrES-1  $5\sigma$  detection at 4.5  $\mu\text{m}$ , taking into account that *JWST* has 40 times the collecting area of *Spitzer* and assuming that the overall efficiency of *JWST* is almost 2x lower, giving an effective collecting area improvement of  $\sim 25$  times. *JWST* will therefore be able to detect hot Jupiter thermal emission at an SNR of 25 around stars at TrES-1’s distance ( $\sim 150$  pc; a distance that includes most stars from shallow ground-based transit surveys). Similarly, *JWST* can detect a hot planet 5 times smaller than TrES-2, or down to 2 Earth radii, for the same set of stars, assuming that instrument systematics are not a limiting factor. Scaling with distance, *JWST* can detect hot Jupiters around stars 5 times more distant than TrES-1 to SNR of 5, which includes all of the *Kepler* and *COROT* target stars. Beyond photometry, *JWST* can obtain thermal emission spectra (albeit at a lower SNR than for photometry of the same planet). Rebinning the  $R=3,000$  NIRSpec data to low-resolution spectra will enable detection of  $\text{H}_2\text{O}$ , CO,  $\text{CH}_4$ , and  $\text{CO}_2$ .

For hot Jupiter transmission spectra, we turn to simulations of NIRSpec transmission spectra [50]. NIRSpec will have three “high-resolution” ( $2200 < R < 4400$ ) gratings (G140H, G235H, G395H) that span the wavelength range 1–5  $\mu\text{m}$ . Observations of planet host stars will be made with the largest fixed aperture ( $4'' \times 0.4''$ ), rather than microshutters. A  $2048 \times 64$  subarray on each of the two detectors will be nondestructively read “up-the-ramp” every 0.3 s for 2.4 s (G140H, G235H) or 3.6 s (G395H). The detector is then reset to avoid charge saturation ( $> 60,000 e^-$ ), and the process is repeated thousands of times to build up 2 hours of total exposure time. The total spacecraft time required to achieve this exposure time depends on the idle time between individual subarray exposures. *JWST* has the potential to characterize the atmospheres of dozens of transiting planets, if overheads and calibration errors can be controlled.

One of us [50] has simulated NIRSpec observations with *JWST*. They estimated NIRSpec performance based on observatory requirements and some lab data. For reference, *JWST* has 25  $\text{m}^2$  clear aperture and a 33% peak efficiency for the NIRSpec/G140H mode considered here. The simulated observations include those in and out of transit, based on NextGen models [51] and planetary absorption spectra from [52]. Simulated noise takes into account the details of how the detector will be read and how spectra will be extracted. (This software is available upon request from valenti@stsci.edu.) [50] do not attempt to estimate the impact of systematic errors that will undoubtedly affect actual observations.

Figure 7 shows a simulation of a  $K = 12$ ,  $V=13.4$  star with a 6 hour observation using NIRSpec/G140H, centered on a 2h planetary transit. Both the theoretical spectra and the simulated observations are shown. In the simulated observation, the water vapor absorption features are obvious and their detection significance is high. This is in contrast to the 3 to 4 SNR transmission spectra detections measured with *HST*, *Spitzer*, and from the ground.

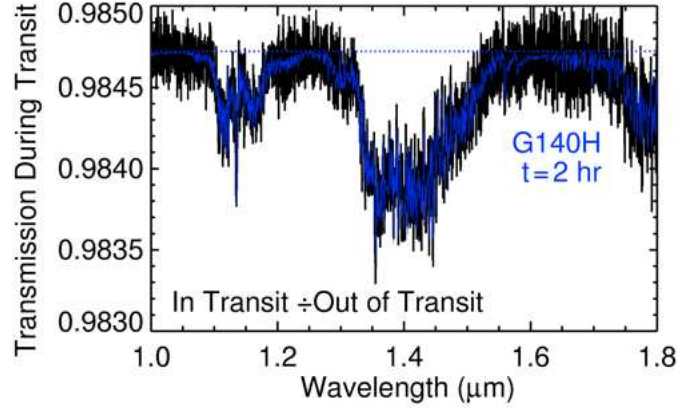


**Fig. 7** Simulated NIRSpec measurements of transmission spectra of a hot Jupiter exoplanet. The spectrum is the ratio of the simulated spectrum in and out of transit. The blue spectrum shows the Brown et al. (2001) model used to generate the simulated observations (black curve). The dominant absorption features are water vapor.

A magnitude of  $V=13.4$  encompasses most stars surveyed in the shallow ground-based transit surveys, which may discover well over 100 hot Jupiters by the time of *JWST*'s launch. *Kepler*'s star magnitude range is  $V=9$  to 16 (most transits will be found around stars  $V=14$  to 16), and therefore the simulated spectrum in Figure 7 applies to *Kepler*'s hot Jupiters as well (although with a slightly lower SNR for the fainter-end stars). By binning NIRSpec data in wavelength, Jupiter transiting planets orbiting out to 1 AU are accessible for NIRSpec transmission spectra. Such observations may help resolve the puzzling question on the origin of the “puffed-up” hot Jupiters that are too large for their mass and age (upper right corner in Figure 5).

Other outstanding questions for hot Jupiters that *JWST* can address include the atmospheric circulation. Tidally-locked to their parent stars, hot Jupiters have a permanent day and night side. By studying the thermal emission spectra as a function of phase we can get a handle on how the temperature of different layers of the planet is changing. Intriguing are the eccentric hot Jupiters whose atmospheres are intensely heated for a brief period of time. Spectra as a function of phase will help us to determine the radiation time constant, a fundamental factor in understanding atmospheric circulation.



By binning NIRSpec data in wavelength, transiting planets smaller than Jupiter can be studied as well. Between Jupiters and super Earths, we expect many hot transiting Neptune-sized exoplanets to be known and accessible to study by *JWST*.

### 4.3 Terrestrial Planet Atmospheres

One of the most interesting exoplanet questions *JWST* can address is whether a planet is habitable. By habitable, we mean, in the conventional sense, one with surface liquid water. Atmospheric water vapor is a good indication of surface liquid water. On Earth,  $O_2$  is considered the most significant biosignature, given that it is a highly reactive gas with a very short lifetime, and only produced in large quantities by biological processes. For signs of life, one would ideally want to observe signatures of molecules that are highly out of redox equilibrium (such as methane and oxygen)[53, 54], but in reality it will be difficult enough to observe any molecular signature robustly from an Earth-temperature, near Earth-size exoplanet. Finally,  $CO_2$ , while not a biosignature, indicates an terrestrial-planet atmosphere. See [55] for a discussion of Earth’s biosignatures.

We choose six examples to illustrate *JWST*’s capabilities for studying terrestrial exoplanets orbiting in their star’s habitable zone.

The first is for a large Earth-like exoplanet. In [42], Gilliland considered a 1.5 Earth-radius planet orbiting a Sun-like star at 1 AU at 20 pc distance. *JWST* could achieve a  $500\text{-}\sigma$  detection with 0.25 sec exposures, 0.5 sec down time, and  $3 \times 10^8$  photons per integration (i.e.,  $10^5$  pixels for 50k electrons in the brightest pixel). This kind of detection can distinguish between Earth- and Venus-like atmospheres. The observations required for such a  $4\text{-}\sigma$  discrimination in this case would span 30 hours centered on a 10-hour transit. This measurement relies on a *JWST* capability of efficiently recording high photon fluxes. More significantly, this hypothetical planet-star system is optimistic; transiting Earths around  $V=6$  dwarfs will be rare and currently no transit survey is capable of finding them.

The second and third examples are for Earth-size planets orbiting M stars. There is new excitement in finding transiting planets orbiting in the habitable zones of M stars. Recall that the habitable zone is defined as the location around a star where a planet’s surface temperature will permit liquid water. Owing to their low luminosity, M stars have habitable zones much closer (3 to 40 day period orbits) than Sun-like stars (1 year orbits). In comparison to the above example of a 1.5 Earth-radius planet in a 1 AU orbit transiting a Sun-like star: the probability to transit is high (transit probability is  $R_*/a$ ); transits are deep; the radial velocity signature is higher and mass measurements are possible; the large planet-star contrast may permit thermal emission measurements. A ground-based targeted transit search for bright M stars is underway [56] and expects to yield a few potentially habitable planets, as are ongoing radial velocity surveys of M stars.

One of us [57] has simulated NIRSpec spectra for transiting Earth-like spectra [58] orbiting bright M stars (Figure 8). Orbiting in the habitable zone ( $P=29$  days)

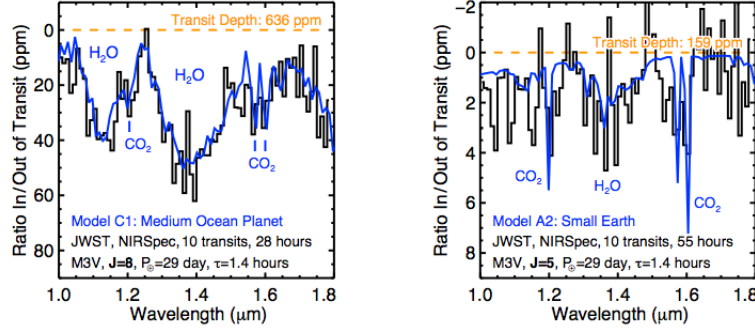


**Fig. 8** Simulated NIRSpec measurements of transmission spectra of habitable exoplanets. The spectra are the ratio of simulated spectra in and out of transit. Details of the planet and star scenarios are indicated on the Figure. The blue spectrum shows the Ehrenreich et al. (2006) models used to generate the simulated observations (black curve). The dominant absorption features are indicated.

of an M3V, J=8 star, an ocean planet will have a strong atmospheric water vapor signature at the level of 40 to 60 ppm. CO<sub>2</sub> features may also be detectable. With a 1.4 hour transit duration, 10 transits and 28 hours of observing time are needed for suitable SNR. This ocean planet example is an  $0.5 M_{\oplus}$ ,  $1 R_{\oplus}$  planet. Its lower density makes its scale height more than 2 times higher than Earth's (Section 4.1) making a transmission spectrum twice as easy to detect (see Section 4.1). For a “small Earth” (defined as 0.1 Earth masses and 0.5 Earth radii) also orbiting in the habitable zone of M3V star (but now for a slightly brighter, J=6 star), the water vapor signatures are several ppm. 54 hours of observing time would be needed for a significant detection. With the period of 29 days in both of these examples, scheduling to observe 10 or more transits is critical. We emphasize that more work both in modeling the planet atmospheres and in *JWST* simulations needs to be done. Regardless, M3V or later stars as bright as J=6 to J=8 are rare, making transiting planets even more rare.

The fourth example is for a super Earth with a hydrogen-rich atmosphere instead of a hydrogen-poor atmosphere. A hydrogen-rich atmosphere would be created by outgassing on a super Earth with a surface gravity high enough to prevent loss of all of the hydrogen. We have described in Section 4.1 how the scale height is inversely proportional to surface gravity and mean molecular weight. We take a  $5 M_{\oplus}$ ,  $1.5 R_{\oplus}$  planet [38] with a corresponding surface gravity 2.2 times higher than Earth's and a mean molecular weight 44 times lower. The transmission spectra signal will be 10 times stronger than the medium ocean planet described in example 2 and Figure 8. Such a hydrogen-rich kind of planet would require  $\sim$  three times less observing time than the Earth-like planet atmosphere in example 2 above, or approximately 10 hours. For further discussion on hydrogen-rich atmospheres on super Earths see [49].

For our final examples, we consider the possibility of mid-IR thermal emission detection during secondary eclipse of an Earth-temperature planet with MIRI. MIRI spectra, in general, may be very useful because with no slit, no detrimental effect

from pointing errors will occur (see Section 2.4). Regarding Earth-type planets, detection of the ozone ( $O_3$ ) and  $CO_2$  spectral features are key (Figure 9).

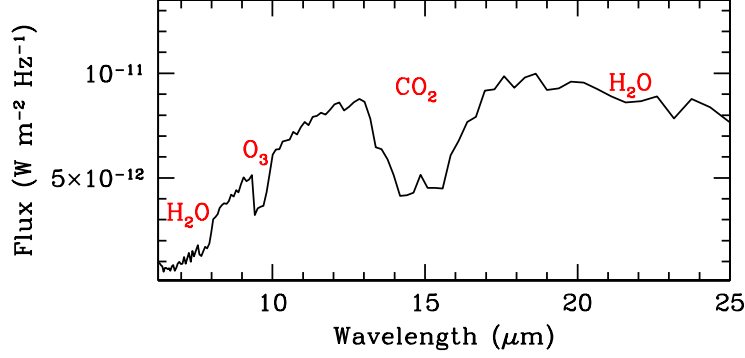


**Fig. 9** Earth's mid-infrared spectrum as observed by Mars Global Surveyor enroute to Mars [59]. Major molecular absorption features are noted.

One of us (Deming) has simulated MIRI observations (also presented in [60] but with minor corrections here). The planet is modeled as a black body in thermal equilibrium with its star, using a Kurucz model atmosphere for the star [61]. Since the star is bright, its statistical photon fluctuations are a dominant noise source. Noise from the thermal background of the telescope and Sun shield, and background noise from zodiacal emission in our solar system are also included. The efficiency of the telescope/MIRI optical system (electrons out / photons in) was taken to be 0.3.

Figure 10 shows the SNR for MIRI R=20 spectroscopy of a  $2 R_{\oplus}$  super Earth orbiting at 0.03 AU around a 20-pc-distant M5V host star as a function of wavelength. Figure 10 aims to show that the SNR would be high enough to detect the  $O_3$  or  $CO_2$  features shown in Figure 9. With a 100 hour observation (for  $\sim 40$  transits and with the total time divided between in-eclipse and out-of eclipse) a SNR of 10 to 15 is possible. Figure 11 shows a similar example, but for a 200 hour observation of a  $1 R_{\oplus}$  planet orbiting in the habitable zone of a 10-pc-distant M8V star with R=50. For comparison, we note that 100 hours is a bit less than half of the Hubble Deep Field observing time.

For both SNR vs. wavelength examples in Figures 10 and 11, the SNR increases at the blue wavelength range due to the increasing number of photons from the planet. At longer wavelengths, the SNR decreases because of greater thermal background noise from the telescope and the Sun shield. Like the above transmission spectra examples, transiting exoplanets suitable for *JWST*/MIRI followup observations of secondary eclipses are anticipated to be rare.

The only *JWST* instrument we have not discussed is NIRCcam, simply due to the current lack of available exoplanet simulations. A brief discussion of transiting

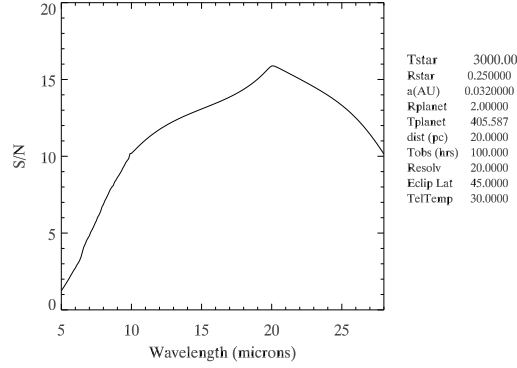


**Fig. 10** MIRI simulation of the SNR as a function of wavelength for R=20 spectroscopy of a  $2 R_{\oplus}$  super Earth orbiting at 0.03 AU around an 20-pc-distant M5V host star (where the planet's  $T_{eq} = 406$  K). The SNR would be high enough to detect the  $O_3$  or  $CO_2$  features shown in Figure 9.

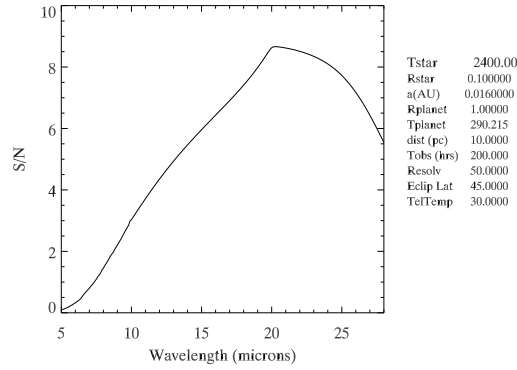


**Fig. 11** MIRI simulation of the SNR as a function of wavelength for R=50 spectroscopy of a  $1 R_{\oplus}$  planet orbiting at 0.016 AU around an 10-pc-distant M8V host star (where the planet's  $T_{eq} = 290$  K). The SNR would be high enough to detect the  $O_3$  or  $CO_2$  features shown in Figure 9.

exoplanet science with the NIRCcam grisms is presented in [62]. NIRCcam will be suitable for both observing primary transit and secondary eclipse. Due to the lack of slit (see Section 2.4), the grisms, and the near-infrared wavelengths where many molecules have absorption features, NIRCcam holds huge promise for transiting exoplanet atmosphere studies.

In summary, *JWST* has the capability to study spectral features of Earth-size or larger planets in the habitable zones of main sequence stars. We need to first find these rare transiting planets and second be patient with the tens to hundreds of hours of *JWST* time with the concomitant complex scheduling to cover periodic transits.

## 5 Discussion

The *Hubble Space Telescope* and the *Spitzer Space Telescope* (Section 2.4) were not designed to achieve the very high SNRs necessary to study transiting exoplanets, but they have succeeded nonetheless. We have learned from these observations that with enough photons, systematics that were unknown in advance can often be corrected for (as long as the errors are uncorrelated). Given the expected thermal stability of *JWST* and the differential nature of transit observations, we are optimistic that *JWST*, too, will succeed in high-contrast transit observations.

We have described a few examples where *JWST* will have a significant impact, including measuring precise exoplanet radii for all sizes of exoplanets and spectra for giant planets at a variety of semi-major axes. Individually, these observations will be “cheap” in terms of telescope time, with single transit measurements being sufficient.

The most significant exoplanet observations *JWST* is poised to make are those for potentially habitable exoplanets. In the most optimistic case, *JWST* is able to identify planets with atmospheric water vapor, or even chemical disequilibrium indicative of biological origin. *JWST* has the capability to do so if the tens to hundreds of hours per target are allocated, and if such rare transiting planets can be discovered in sufficient numbers.

**Acknowledgements** We thank Mark Clampin, George Ricki, Dave Charbonneau, and Heather Knutson for useful discussions.

## References

1. <http://exoplanet.eu/>
2. Butler, R. P. et al. 2006, *ApJ*, 646, 505
3. Udry, S., Fischer, D., & Queloz, D. 2007, *Protostars and Planets V*, 685
4. Charbonneau, D., Brown, T. M., Burrows, A., & Laughlin, G. 2007, *Protostars and Planets V*, 701
5. Gaudi, B. S., et al. 2008, *Science*, 319, 927
6. Chauvin, G., Lagrange, A.-M., Dumas, C., Zuckerman, B., Mouillet, D., Song, I., Beuzit, J.-L., & Lowrance, P. 2004, *A&A*, 425, L29
7. Wolszczan, A., & Frail, D. A. 1992, *Nature*, 355, 145
8. Silvotti, R., et al. 2007, *Nature*, 449, 189
9. Chauvin, G., et al. 2005, *A&A*, 438, L29
10. Neuhäuser, R., Guenther, E. W., Wuchterl, G., Mugrauer, M., Bedalov, A., & Hauschildt, P. H. 2005, *A&A*, 435, L13
11. Gardner, J. P., et al. 2006, *Space Science Reviews*, 123, 485
12. Fazio, G. G., et al. 2004, *ApJS*, 154, 10
13. Houck, J. R., et al. 2004, *ApJS*, 154, 18
14. Rieke, G. H., et al. 2004, *ApJS*, 154, 25
15. Richardson, L. J., Harrington, J., Seager, S., & Deming, D. 2006, *ApJ*, 649, 1043
16. Butler, R. P., Vogt, S. S., Marcy, G. W., Fischer, D. A., Wright, J. T., Henry, G. W., Laughlin, G., & Lissauer, J. J. 2004, *ApJ*, 617, 580

17. Gillon, M., et al. 2007, *A&A*, 472, L13
18. Deming, D., Harrington, J., Laughlin, G., Seager, S., Navarro, S. B., Bowman, W. C., & Horning, K. 2007, *ApJ*, 667, L199
19. Gillon, M., et al. 2007, *A&A*, 471, L51
20. Cox, A. N. 2000, *Allen's astrophysical quantities*, 4th ed. Publisher: New York: AIP Press; Springer, 2000. Edited by Arthur N. Cox. ISBN: 0387987460
21. Knutson, H. A., et al. 2007, *Nature*, 447, 183
22. Deming, D., Seager, S., Richardson, L. J., & Harrington, J. 2005, *Nature*, 434, 740
23. Harrington, J., Hansen, B. M., Luszcz, S. H., Seager, S., Deming, D., Menou, K., Cho, J. Y.-K., & Richardson, L. J. 2006, *Science*, 314, 623
24. Cowan, N. B., Agol, E., & Charbonneau, D. 2007, *MNRAS*, 379, 641
25. Seager, S., Richardson, L. J., Hansen, B. M. S., Menou, K., Cho, J. Y.-K., & Deming, D. 2005, *ApJ*, 632, 1122
26. Harrington, J., Luszcz, S., Seager, S., Deming, D., & Richardson, L. J. 2007, *Nature*, 447, 691
27. Burrows, A., Budaj, J., & Hubeny, I. 2008, *ApJ*, 678, 1436
28. Fortney, J. J., Lodders, K., Marley, M. S., & Freedman, R. S. 2007, *ArXiv e-prints*, 710, arXiv:0710.2558
29. Showman, A. P., Menou, K., & Y.-K. Cho, J. 2007, *ArXiv e-prints*, 710, arXiv:0710.2930
30. Hubeny, I., Burrows, A., & Sudarsky, D. 2003, *ApJ*, 594, 1011
31. Charbonneau, D., et al. 2005, *ApJ*, 626, 523
32. Burrows, A., Hubeny, I., Budaj, J., Knutson, H. A., & Charbonneau, D. 2007, *ApJ*, 668, L171
33. Knutson, H. A., Charbonneau, D., Allen, L. E., Burrows, A., & Megeath, S. T. 2008, *ApJ*, 673, 526
34. Tinetti, G., et al. 2007, *Nature*, 448, 169
35. Ehrenreich, D., Hébrard, G., Lecavelier des Etangs, A., Sing, D. K., Désert, J.-M., Bouchy, F., Ferlet, R., & Vidal-Madjar, A. 2007, *ApJ*, 668, L179
36. Morales-Calderón, M., et al. 2006, *ApJ*, 653, 1454
37. Deming, D., & Seager, S., submitted to *ApJ*
38. Seager, S., Kuchner, M., Hier-Majumder, C. A., & Militzer, B. 2007, *ApJ*, 669, 1279
39. Valencia, D., Sasselov, D. D., & O'Connell, R. J. 2007, *ApJ*, 665, 1413
40. Zeng and Seager, *PASP*, in press
41. Brown, T. M., Charbonneau, D., Gilliland, R. L., Noyes, R. W., & Burrows, A. 2001, *ApJ*, 552, 699
42. Seager and Lunine, eds. *JWST and Astrobiology white paper*, NASA Astrobiology Institute
43. Beichman, C. A., Fridlund, M., Traub, W. A., Stapelfeldt, K. R., Quirrenbach, A., & Seager, S. 2007, *Protostars and Planets V*, 915
44. Basri, G., Borucki, W. J., & Koch, D. 2005, *New Astronomy Review*, 49, 478
45. Charbonneau, D., Brown, T. M., Noyes, R. W., & Gilliland, R. L. 2002, *ApJ*, 568, 377
46. Swain, M. R., Vasisht, G., & Tinetti, G. 2008, *Nature*, 452, 329
47. Vidal-Madjar, A., Lecavelier des Etangs, A., Désert, J.-M., Ballester, G. E., Ferlet, R., Hébrard, G., & Mayor, M. 2003, *Nature*, 422, 143
48. Redfield, S., Endl, M., Cochran, W. D., & Koesterke, L. 2008, *ApJ*, 673, L87
49. Miller-Ricci, Seager, Sasselov, submitted to *ApJ*
50. Valenti, J. A., et al. 2005, *Bulletin of the American Astronomical Society*, 37, 1350
51. Hauschildt, P. H., Allard, F., & Baron, E. 1999, *ApJ*, 512, 377
52. Brown, T. M. 2001, *ApJ*, 553, 1006
53. Lederberg, J. 1965, *Nature*, 207, 9
54. Lovelock, J. E. 1965, *Nature*, 207, 568
55. Des Marais, D. J., et al. 2002, *Astrobiology*, 2, 153
56. Nutzman, P., & Charbonneau, D. 2007, *ArXiv e-prints*, 709, arXiv:0709.2879
57. Valenti, J. A., Turbull, M., McCullough, P., & Gilliland, R. 2008, in prep.
58. Ehrenreich, D., Tinetti, G., Lecavelier Des Etangs, A., Vidal-Madjar, A., & Selsis, F. 2006, *A&A*, 448, 379
59. Christensen, P. R., & Pearl, J. C. 1997, *JGR*, 102, 10875
60. Charbonneau, D., & Deming, D. 2007, *ArXiv e-prints*, 706, arXiv:0706.1047
61. Kurucz, R. L. 1992, *The Stellar Populations of Galaxies*, 149, 225
62. Greene, T., et al. 2008, *SPIE*, in press